A Study on the Production Performance of a Horizontal Shale Gas Well Using a Fully Coupled Flow and Geomechanics Modelling

Tareq Mohammed Al-Shami[1], Shiferaw Regassa Jufar[1,*], Mohammed Bashir Abdullahi[1], Berihun Mamo Negash[1]

[1]   Department of Petroleum Engineering, Universiti Teknologi PETRONAS, Seri Iskandar, Malaysia

ARTICLE INFO	ABSTRACT
	Conventional petroleum reservoir simulators use constant rock compressibility to denote rock deformation. However, due to the stress-sensitive nature of the shale formations, using constant rock compressibility in reservoir simulators does not accurately capture the pressure diffusion in the reservoir, leading to a higher error margin in flow rate estimation. Fluid flow coupling with geomechanics is used to account for such a phenomenon numerically. Such an approach is important for shale numerical studies and any energy underground storage modeling (i.e., CO_2 storage). Usually, when fluid flow coupling with geomechanics is studied for shale formations, the fluid, and the stimulated reservoir petrophysical properties are overlooked. This paper aims to present a study on the effect of the fluid and reservoir petrophysical properties on the performance of a gas-producing well. In addition, the results from the cases when geomechanics is coupled and decoupled with fluid flow in reservoir simulations are compared. The governing equations were discretized using the Finite Element Method. First, the model was validated against Terzaghi's consolidation theory analytical solution. After that, a history matching for the production flow rate was performed using field production data from Barnett Shale. Then a sensitivity analysis was carried out for the gas viscosity, Stimulated Reservoir Volume (SRV) porosity, and fracture conductivity. Next, the sensitivity analysis was conducted for the coupled and decoupled cases. Finally, the sensitivity analysis results were compared between the coupled and decoupled cases. The results show that lower gas viscosity, higher SRV porosity, and higher fracture conductivity improved horizontal well production performance. In addition, when the geomechanical effects were decoupled, the reservoir simulator overestimated the production flow rate and cumulative production.

1. Introduction

Fossil energy, specifically hydrocarbons, remains the main energy source worldwide [1–4]. Hydrocarbons can be produced in the form of gases or oil and can be produced from conventional and unconventional reservoirs [5–7]. The rocks that contain conventional hydrocarbon resources (e.g., sandstone) are well-known for having good porosity and permeability [8]. As a result, these

___
* *Corresponding author.*
E-mail address: Shiferaw.jufar@utp.edu.my

reservoir rocks do not need stimulation for hydrocarbon production. However, the rocks that contain unconventional hydrocarbon resources (e.g., shale rocks) are known for having extremely low permeability [9–12]. As a result, producing hydrocarbons from such reservoirs would require stimulation intervention (e.g., hydraulic fracturing) [13,14]. Due to the depletion of conventional hydrocarbon resources and the scarcity of new conventional reservoir discoveries, stimulating the rocks that contain the unconventional resources and producing them became viable [15–18]. Additionally, the newly developed techniques of drilling long horizontal wells that are completed with multi-stage hydraulic fracturing resulted in a significant production increment from shale reservoirs worldwide [19–22].

Shale rock formations contain natural fractures that may act as conduits for hydrocarbon recovery [23]. In addition to the natural fractures, the shale rock formations are stimulated with multi-stage hydraulic fracturing. Multi-stage hydraulic fracturing in horizontal wells creates a large stimulated reservoir volume (SRV). SRV is the key contributor to high hydrocarbon production from shale reservoirs [24–27]. The combination of natural fractures, hydraulic fractures, and the relatively low consolidation of the shale rocks make the shale formations sensitive to changes in the in-situ stresses [28,29]. As a result, the shale formations are well-known for being stress sensitive [30, 31]. It is important to note that any change in the stress fields would alter the porosity and permeability and possibly cause failures and fracture development or closures; hence these processes can influence the flow pattern of the whole system [32,33]. Thus, having a greater insight into the effect of geomechanics on fluid flow would yield useful information about petroleum reservoir modeling and simulation.

Conventional reservoir simulators use a constant rock compressibility factor to denote the basic rock deformation process. However, geomechanics coupled with fluid flow simulations should be utilized for better accuracy in stress-sensitive formations. Modeling of geomechanics coupling with fluid flow in porous media can be achieved by applying the consolidation theories in reservoir rocks. The idea of effective stress in consolidation was first introduced by Terzaghi [34,35], providing a useful framework for investigating fluid and rock interaction. Additionally, Biot's theory of poroelasticity is the most widely used theory to explain the poromechanical interaction [36–38]. Moreover, Greetsma [39] was the first to present a unified treatment of rock mechanics in petroleum production engineering. The use of geomechanics coupling with the fluid flow is important in any numerical modeling that is affected by poroelasticity, such as CO_2 storage [40–42].

The fluid flow coupling with geomechanics has gained significant attention lately. The effect of the mechanical rock properties and hydraulic fracture geometry on the fluid flow has been studied extensively [28,30,33,43–48]. However, when such a numerical approach is utilized, the effect of the SRV petrophysical parameters and fluid properties are under-investigated. As a result, this paper aims to study the effect of the SRV petrophysical parameters and fluid properties on the production performance of a gas-producing horizontal well that is completed with multi-stage hydraulic fracturing. In addition, this paper aims to show the difference between the cases when the geomechanics effects are coupled with the reservoir simulator and when it is decoupled. The petrophysical parameters and the fluid property that are studied in this paper are the SRV porosity, the hydraulic fracture conductivity, and the gas viscosity.

2. Methodology

This study uses a fully coupled fluid flow and geomechanics model. The fluid flow is isothermal single-phase gas that assumes a Darcy flow throughout the domain. The geomechanics is solved using linear elasticity, assuming isotropic rock material. The fluid flow equations are governed by the mass

balance (the continuity equation) and Darcy equation, while the geomechanics equations are governed by the equilibrium equation.

2.1 Governing Equations

Assuming a transient flow, the governing equation for a single-phase fluid flow in porous media assuming an infinitesimal rock deformation can be described by

$$\left(\frac{b-\phi}{K_s} + \phi c_g\right)\frac{\partial p}{\partial t} + b\frac{\partial \varepsilon_v}{\partial t} + \nabla.q = f \tag{1}$$

where b is Biot's coefficient, ϕ is the porosity, K_s is the rock solid grain bulk modulus, c_g is the gas phase compressibility, p is the pore pressure, ε_v is the volumetric strain, q is the gas flow rate accounting for gas fluxes, and f is the sink/source term of the gas.

In the fluid flow governing Eq. (1), Darcy's law is used in the calculation of the flux term for gas [49]. Darcy's law can be described as

$$q = \frac{k}{\mu}.\left[-\nabla p + \rho_g\vec{g}\right] \tag{2}$$

where k is the second-order permeability tensor, μ is the gas viscosity, and $\vec{g}$ is the gravitational acceleration vector. Isotropic permeability is assumed because permeability anisotropy is beyond the scope of this study. As a result, a single value for the permeability is used.

The geomechanical deformation is calculated based on the equilibrium equation that is described as

$$\nabla.\boldsymbol{\sigma} + \rho_b\vec{g} = 0 \tag{3}$$

where $\boldsymbol{\sigma}$ is the Cauchy total-stress tensor, and ρ_b is the total bulk density. Following the typical geomechanics convention, the compressive stress is denoted as positive. Using Biot's theory of consolidation [38], the total stress can be expressed as

$$\boldsymbol{\sigma} = \boldsymbol{\sigma_0} - \boldsymbol{\sigma}' + bp\boldsymbol{I} \tag{4}$$

where $\boldsymbol{\sigma_0}$ is the initial stress tensor, $\boldsymbol{\sigma}'$ is the effective stress tensor, and $\boldsymbol{I}$ is the second-order identity tensor. The effective stress is given by the constitutive relation described as

$$\boldsymbol{\sigma}' = C:\varepsilon \tag{5}$$

where C is the fourth-rank rock stiffness tensor, and ε is the rock strain rate tensor. The rock strain rate tensor is related to the solid displacement $\vec{u}$ by

$$\varepsilon = \frac{1}{2}(\nabla\vec{u} + (\nabla\vec{u})^T) \tag{6}$$

Eq. (1), Eq. (2), and Eq. (3) are the three governing equations that are solved in one system for the full fluid flow coupling with the geomechanics model.

2.2 Numerical Model

The three governing equations are discretized using the finite element method. Three test functions are used to write the weak form of the governing equations (P_w, Q_w, U_w). The numerical solution for the pore pressure p, flow rate q, and solid displacement $\vec{u}$ are P_h, q_h and $\vec{u}_h$ respectively. The discretized solutions are solved in the spaces: Discontinuous Galerkin DG × Raviart–Thomas RT × Continuous Galerkin CG, respectively. The three governing equations are solved monolithically using the mixed finite element method. The combination of finite element types for these function spaces has been selected because their solution has shown to be stable [45, 50–53].

Using the traditional Galerkin method, the weak form of the governing equations is given below

$$\int_\Omega \left(\frac{b-\emptyset}{K_s}+\emptyset c_g\right)\frac{p^{n+1,m+1}-p^n}{\Delta t}P_w d\Omega + \int_\Omega b\frac{\nabla.\vec{u}^{n+1,m+1}-\nabla.\vec{u}^n}{\Delta t}P_w d\Omega$$

$$+\int_\Omega \nabla.q^{n+1,m+1}P_w d\Omega = \int_\Omega f\,P_w d\Omega \tag{7}$$

$$\int_\Omega \frac{\mu}{k}q^{n+1,m+1}.Q_w d\Omega = \int_\Omega q^{n+1,m+1}\nabla.Q_w d\Omega - \int_\Gamma p^{n+1,BC}n.Q_w d\Gamma + \int_\Omega \rho_g\vec{g}\,Q_w d\Omega \tag{8}$$

$$\int_\Omega \sigma^{n+1,m+1}.\nabla U_w d\Omega + \int_\Omega \rho_b\vec{g}.U_w d\Omega = \int_\Gamma (t^{n+1,BC}.n).U_w\,d\Gamma \tag{9}$$

where Ω denotes the domain, Γ denotes the boundary, Δt is the time step size, the superscripts n and $n+1$ represent the previous and current time steps respectively, the superscripts m and $m+1$ represent the previous and current Picard iterations respectively, $t^{n+1,BC}$ and $p^{n+1,BC}$ are the stipulated traction and pressure boundary conditions.

Due to pore pressure reduction, effective stress will be altered, leading to rock consolidation, thus altering the porosity and permeability [54–58]. As a result, after the pore pressure and solid displacement solutions are obtained, for higher solution accuracy, the porosity is updated using Biot & Willis [36] and Geertsma [39] consolidation theory. Additionally, the exponential porosity-dependent permeability developed by Davies and Davies [59] is adopted to update the permeability. The initial conditions are given by

$$P_0 = P_i \tag{10}$$

$$q_0 = 0 \tag{11}$$

$$\vec{u}_0 = 0 \tag{12}$$

where P_0 is the initial pore pressure, q_0 is the initial flow rate, and $\vec{u}_0$ is the initial rock displacement. The initial condition of the pressure is given in Table 2. The flow rate and the rock displacement are assumed to be zero at the beginning time of the simulation. The six boundaries shown in Figure 2(a) are no flow boundaries. In addition, the vertical stress S_v is applied on the top boundary, as shown in Figure 2(a). The model's bottom, right, left, back and front boundaries are assumed to be fixed boundaries where rock displacement is not allowed.

The time derivative is discretized with a backward Euler scheme. The Picard iterations are employed to handle the model's non-linearity (e.g., porosity and permeability). FEniCS Project is used to solve the system of the partial differential equations of the fluid flow coupling with geomechanics

[60]. FEniCS Project is an open-source Finite Element library with high-level Python and C++ interfaces [60]. FEniCS Project uses several advances in automated Finite Element methodologies, including but not limited to DOLFIN [61], FIAT [62], FFC [63], and UFL [64]. PETSc is the default linear algebra backend for FEniCS Project [65].

2.3 Validation

Terzaghi's classical one-dimensional problem is considered a validation benchmark for consolidation numerical studies because it is the simplest nontrivial application of the theory of consolidation [35, 66, 67]. This problem considers a one-dimensional sample of a vertical column of height H of clay confined with a steel ring. In the absence of gravity, this vertical column has a certain porosity and is fully saturated with a certain fluid. The top of the column is suddenly loaded with a load t at time $t = 0$ s and then kept constant throughout the rest of the time. While the bottom boundary is fixed and is not allowed to drain, the top boundary is a free surface and is allowed to drain. Initially, the domain is undisturbed, and the pore pressure P_i is zero Pascal throughout the whole domain. A schematic of the problem is illustrated in Figure 1(a). The boundaries Γ_1 and Γ_3 are no flow and no displacement boundaries, while the load t is applied at the boundary Γ_2, and it is a flow boundary (free surface) with pressure $p = 0$ Pa. The one-dimensional data is collected along the dashed line shown in Figure 1(a). The properties used in the validation are mentioned in Table 1.

Table 1
Fluid and rock parameters

Parameter	Value
Permeability (k)	10^{-14} m^2
Porosity ($\varnothing$)	0.05
Fluid viscosity (μ)	8.9×10^{-4} Pa.s
Fluid compressibility (c_g)	4.4×10^{-10} Pa
Rock Bulk modulus (K)	10^{10} Pa
Solid grain bulk modulus (K_s)	10^{11} Pa
Poisson ratio (v)	0.25
Traction (t)	5.0×10 Pa

The analytical solution to Terzaghi's one-dimensional problem for the dimensionless pore pressure is given by

$$\frac{p}{p_0} = \frac{1}{4}\sum_{j=1}^{\infty}\left(\frac{1}{2j-1}\sin\left[\frac{(2j-1)\pi}{2H}z\right] \times exp\left[-\left(\frac{[2j-1]\pi}{2H}\right)c_v t\right]\right) \tag{13}$$

where p_0 is the undrained response for the pore pressure throughout the domain, and c_v is the consolidation coefficient given by

$$c_v = \frac{k}{\mu(b^2 m_v + S_\epsilon)} \tag{14}$$

where m_v is the confined compressibility of the porous medium, S_ϵ is the drained storage coefficient.
The dimensionless time is given by

$$t^* = \frac{c_v t}{H^2} \tag{15}$$

In the beginning, the load is applied at the top boundary, and it causes the clay column to consolidate. The consolidation causes a sudden rise in the pore pressure. This sudden increase in the pore pressure causes the fluid to flow towards the low pore pressure regions at the top boundary. As the fluid flows out of the domain, the pore pressure falls steadily until it reaches zero. Once the pore pressure is zero throughout the domain, the consolidation stops, and the clay column goes into equilibrium again. Figure 1(b) shows a comparison between Terzaghi's one-dimensional problem analytical solution (solid line) and the numerical solution (circles). The *y*-axis represents the dimensionless length *z/H* of the clay column, and the *x*-axis represents the dimensionless pore pressure. The analytical solution of the dimensionless pore pressure is the result of Eq. (13), and the numerical solution is the data gathered along the dashed line illustrated in Figure 1(a). The pressure data were collected at different simulation times. It is clear that the numerical solution matches the analytical solution. Therefore, the numerical model seems to produce accurate results.
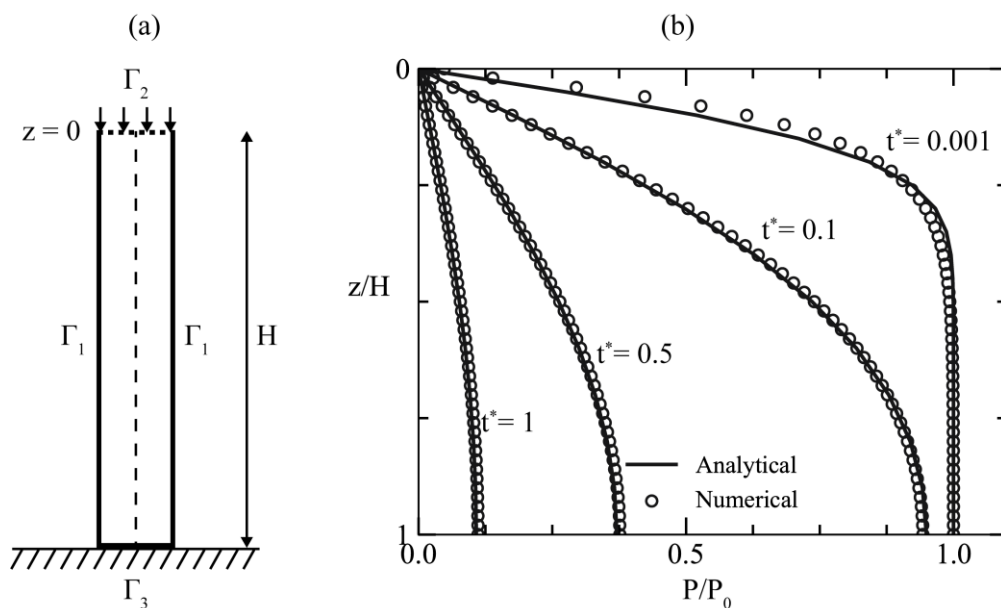

Fig. 1. (a) Side view schematic of Terzaghi's problem, (b) Comparison of Terzaghi's one-dimensional analytical solution with the numerical solution for the top drain boundary case

2.4 History-Matching

The data from Barnett shale is used to construct the reservoir model. The fluid, reservoir, and production input are based on available data from the literature; Song *et al.,* [68] and Gou *et al.,* [45]. The geomechanics data for the model is based on data from Vermylen [69], Yu and Sepehrnoori [70], and Zoback [71]. The production data was used for model calibration and history matching. Table 2 presents the model data in detail. Figure 2(a) shows the model dimensions of the multi-stage discrete hydraulic fractures that were used to investigate the performance of the horizontal well. Data in Table 2 is used to match the production history shown in Figure 2(b).

Figure 2(b), shows the history-matching results. The *y*-axis represents the gas flow rate at reservoir conditions, while the *x*-axis represents the production time. In Figure 2(b), the circles represent the data gathered from a gas producing well in Barnett Shale [68]. The numerical results when the geomechanical effects were coupled with the reservoir simulator are represented by the solid line, while the numerical results when the geomechanical effects were decoupled from the reservoir simulators are represented by the dotted line. The production data gathered from the field seem noisy

due to unknown production conditions. However, the field data exhibits a clear production profile. Therefore, the numerical models (coupled and decoupled) seem to match the production profile exhibited by the filed production data. While the decoupled numerical model seems to overestimate the production flow rate compared to the field production data, it is important to note that the coupled numerical model matches the field production data more accurately. Since the history matching has been achieved, the numerical analysis can be carried out.

Table 2
Fluid, reservoir, and rock parameters for history matching

| Parameter(s)	Value(s)	Unit
Initial reservoir pressure	26.9 (3901.5)	MPa (Psi)
Bottom hole pressure	3.4 (493.13)	MPa (Psi)
Gas Viscosity	2.01×10^{-5} (0.02)	Pa.s (cP)
Matrix permeability	9.87×10^{-19} (1)	m^2 (μD)
Permeability of SRV	4.93×10^{-17} (50)	m^2 (μD)
Matrix porosity	15	%
Porosity of SRV	6.5	%
Fracture conductivity	1.35×10^{-15} (4.5)	m^2-m (md-ft)
Fracture half-length	46 (151)	m (ft)
Fracture Spacing	73 (239.5)	m (ft)
Fracture stages	6	-
Bulk density	2.58×10^3 (161.1)	Kg/m^3 (lb/ft^3)
Biot's coefficient	1	-
Young's modulus	40 (5.8×10^6)	GPa
Poisson's ratio	0.25	-
Vertical Stress	44 (6381.6)	MPa (Psi)
Maximum horizontal stress	29 (4206)	MPa (Psi)
Minimum horizontal stress	28 (4061)	MPa (Psi)
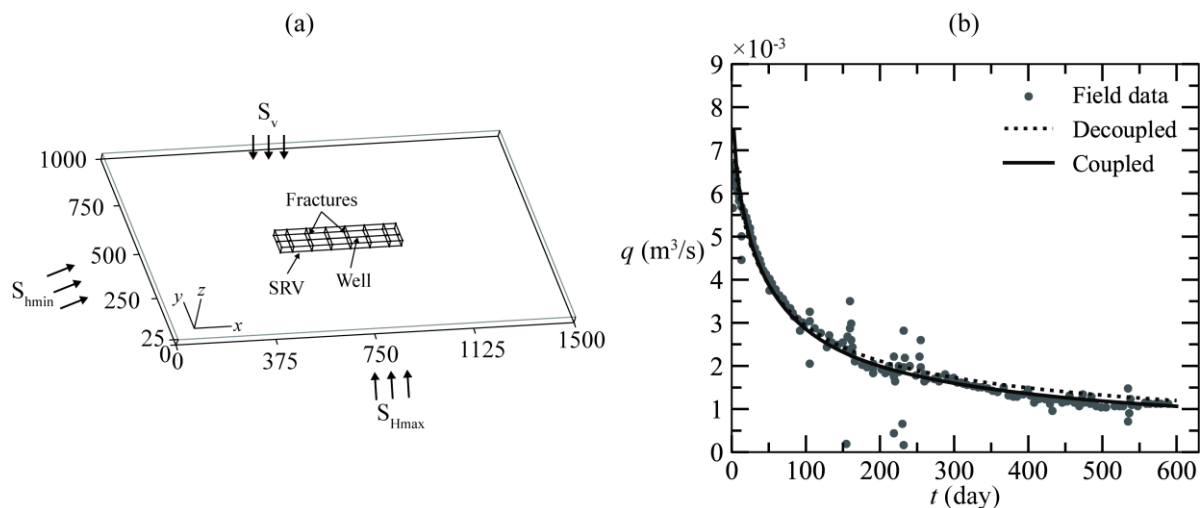
Fig. 2. (a) The model schematic, (b) history matching of the numerical model (coupled and decoupled) with the field data

3. Results and Discussion
3.1 Production History

Figure 3(a) shows a comparison of the reservoir flow rate between the cases when the geomechanical effects were coupled (solid line) with the reservoir simulator and when it was decoupled (dotted line). In Figure 3(a), the *y-axis* represents the reservoir flow rate, and the *x-axis*

represents the time. The production data shown in Figure 3(a) showed the production profile when the well was produced for 600 days. In the first 50 days of production, there was a sharp decline in the flow rate due to the shale rock's low permeability nature. In the first 50 days of production, the flow rate resulting from the coupled and the decoupled numerical cases appears to be the same. However, the production profile beyond the first 50 days seems to differ slightly in the coupled and the decoupled cases. The reason for that is the consideration of rock deformation in the coupled case. As a result of the pore pressure reduction, the effective stress increases [71, 72]. The increment in the effective stress results in rock deformation, thus altering the porosity and permeability. This alteration in the porosity and permeability is reflected by the slight reduction in the flow rate when the geomechanical effects are coupled. In Figure 3(a), the difference in flow rate between the coupled and the decoupled cases do not seem to be significant.

Figure 3(b) shows the same comparison between the coupled and the decoupled cases but for the cumulative production (N_p). In Figure 3(b), the *y-axis* represents the cumulative production while the *x-axis* represents the time. Although the difference in production flow rate was insignificant, the cumulative production for 600 days that resulted from the coupled and the decoupled cases seem to be more notable. When the geomechanical effects were decoupled, the reservoir simulator overestimated the cumulative production by 11% compared to the simulation case when the geomechanical effects were coupled.

Figure 3(c) shows the pore pressure in the third fracture along a 1-dimensional line extended in the *y* direction. The third fracture was chosen in this analysis because, as shown in the pore pressure contour, the pressure depletion seems to be higher in the third and fourth fractures, as shown in Figure 4. In Figure 3(c), the pore pressure for the coupled and the decoupled cases are the same along the third fracture. However, when reaching toward the well, there appears to be a slight difference. The pore pressure depletion in the coupled case is higher than that of the decoupled case. One would expect that the pore pressure of the coupled case would be higher than that of the decoupled case due to the lower flow rate and cumulative production shown in Figures 3(a) and (b)—however, the pore pressure profile shows the opposite of that. The reason for this is that due to the rock deformation in the coupled case, the porosity was reduced, resulting in a faster depletion of the pore pressure.

Figures 4(a) and (b) show a top planer view of the pore pressure contour after 600 days of production for the decoupled and coupled numerical cases, respectively. The contour shown in Figures 4(a) and (b) are cropped from the original model shown in Figure 2(a) because significant pore pressure depletion occurs mostly at the SRV area, as also shown in Figure 3(c). Both coupled and decoupled cases show the pore pressure depletion propagation in the domain in a ripple effect manner. It is important to note that the pore pressure reduction along the six fractures seems more prominent than the rest of the SRV area and the reservoir matrix. Generally, the pore pressure contours show a more significant pore pressure depletion when the geomechanical effects were coupled with the reservoir simulator.
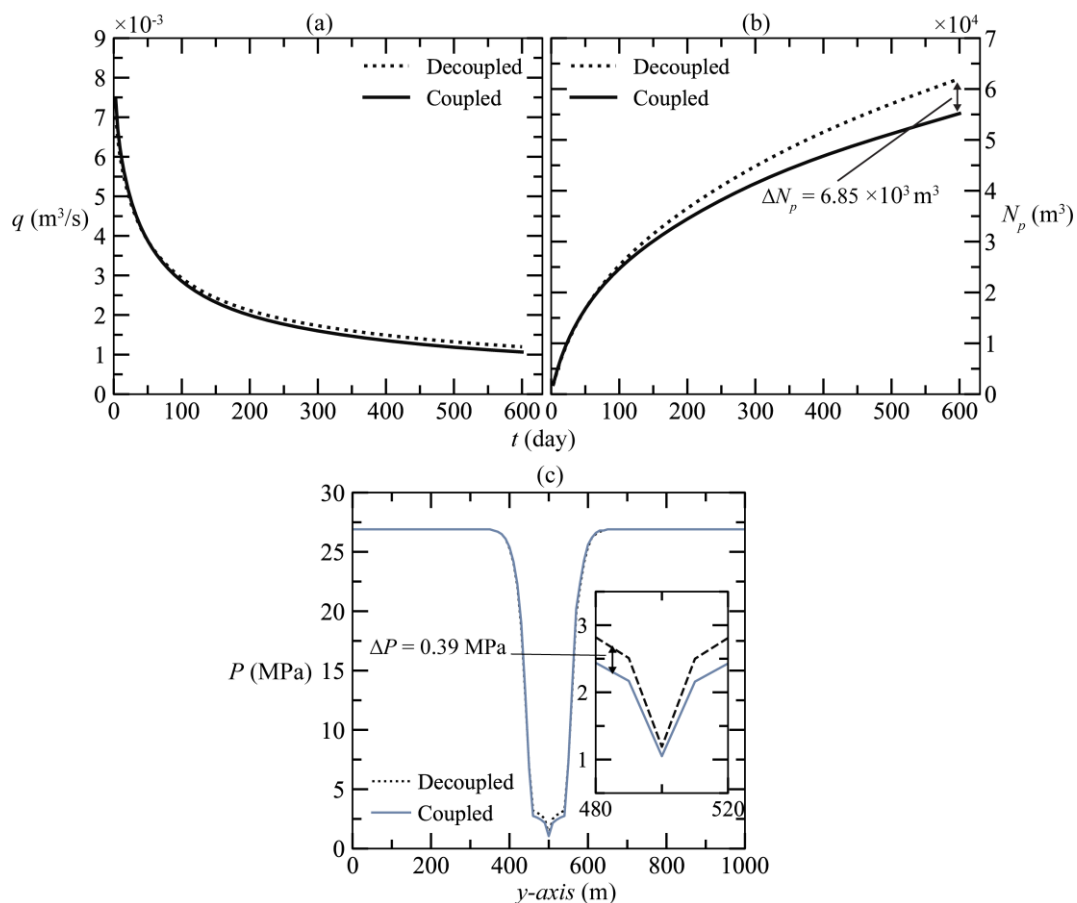
Fig. 3. (a) flow rate for the coupled vs. decoupled cases, (b) a comparison of the cumulative production between the coupled and the decoupled cases, and (c) a comparison of the pore pressure along the third fracture between the coupled and the decoupled cases
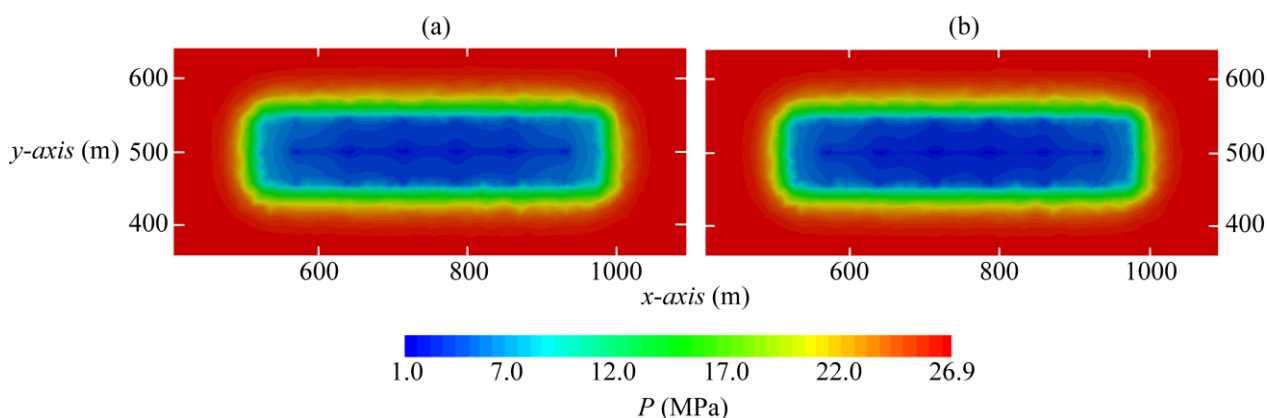
Fig. 4. Pore pressure contour for (a) the decoupled case and (b) the coupled case

3.2 Sensitivity Analysis

After the difference between the cases when the geomechanical effects were coupled with the reservoir simulator and when it was decoupled was shown, this section discusses the sensitivity analysis of the effect of the gas viscosity, the SRV porosity, and the fracture conductivity on the production performance of the horizontal well. The values of the sensitivity analysis for the chosen parameters are within the typical shale gas producing well range [68, 73–76]. This section also shows

the horizontal well production performance when simulated using the coupled and decoupled cases. Table 3 shows the sensitivity analysis parameters used in this study. The base case means the properties mentioned in Table 2 and discussed in section 3.1.

Table 3
The sensitivity analysis parameters

Parameter	Base case	μ (Pa.s)	$\emptyset_{SRV}$ (%)	C_f m^2-m (md-ft)
μ Pa.s	2.01×10^{-5}	2.51×10^{-5} 1.51×10^{-5}	Base case	Base case
$\emptyset_{SRV}$ %	0.065	Base case	0.035 0.095	Base case
C_f m^2-m (md-ft)	1.35×10^{-15} (4.56)	Base case	Base case	2.57×10^{-15} (8.66) 1.35×10^{-16} (0.456)

3.2.1 Gas viscosity

Figure 5 shows the gas viscosity sensitivity analysis. The base case in Figures 5(a) and (a*) refer to the decoupled and coupled cases shown in Figure 3(a), respectively. Figures 5(a) and (a*) show the production flow rate for the case when the geomechanical effects were decoupled and coupled, respectively. Overall, when the gas viscosity was reduced, the production flow rate increased, and vice versa when the gas viscosity was increased. However, the magnitude of the difference between the high and low gas viscosities with respect to the base case is different in the decoupled and coupled cases. In Figures 5(a) and (a*), the difference between the coupled and decoupled cases seems insignificant.

Figures 5(b) and (b*) show a clear difference between the decoupled and coupled cases, respectively. Figures 5(b) and (b*) show the cumulative production for the gas viscosity sensitivity analysis for the decoupled and coupled cases, respectively. Figures 5(b) and (b*) show that the decoupled case overestimated the cumulative production in all the cases of the gas viscosity sensitivity analysis. For the decoupled case, the difference between the low viscosity case (1.51×10^{-5}) and the base case is about 5.96×10^3 m^3 which is about a 14.7% increment in the cumulative production when compared to the base case. However, for the coupled case, the difference between the low viscosity case and the base case is about 4.81×10^3 m^3 which is about a 14.1% increment in the cumulative production compared to the base case. In Figure 3(b), the difference between the coupled and decoupled cumulative production was 6.85×10^3 m^3; however, the difference between the coupled and decoupled cumulative production for the low viscosity case is about 8.30×10^3 m^3. This shows that as the gas viscosity decreases, the decoupled simulator overestimates the cumulative production further. For the high viscosity cases, the difference between the decoupled base case and the higher viscosity case is about 9.12×10^3 m^3 which is about a 9.61% decrement from the base case. However, for the coupled case, the difference between the base case and the higher viscosity case is about 7.78×10^3 m^3 which is about an 8.71% decrement from the base case. This shows that the decrement in the coupled case is not as significant as in the decoupled case. The difference between the base case and the higher and lower viscosity cases for the decoupled cases is much greater than that of the coupled cases.
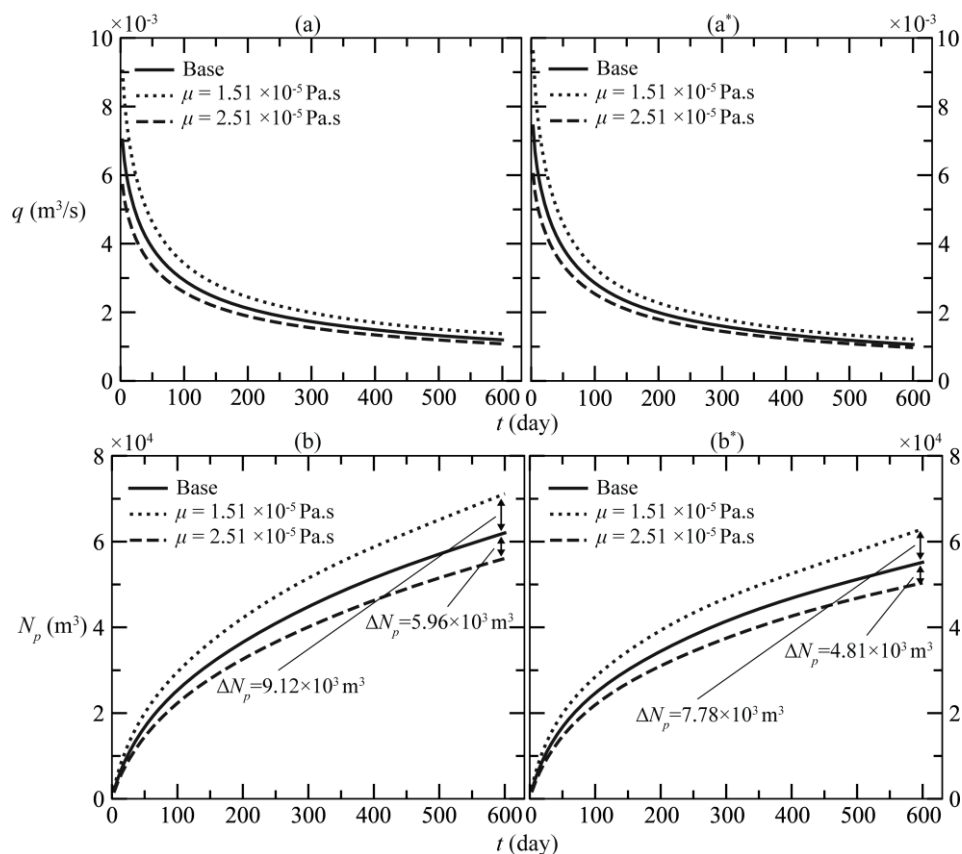
Fig. 5. Gas viscosity sensitivity analysis, (a) the flow rate of the decoupled case, (a*) the flow rate for the coupled case, (b) the cumulative production for the decoupled case, and (b*) the cumulative production for the coupled case

Figure 6(a) and (a*) show the pore pressure of the gas viscosity sensitivity analysis along the third fracture after 600 days of production for the decoupled and coupled cases, respectively. Overall, the pore pressure for the coupled cases seems to be less than that of the decoupled cases. The difference between the higher and lower gas viscosity and the base case for the coupled case seems to be the same at 0.51 MPa. However, the production flow rate and the cumulative production show that the difference ratio between the lower viscosity case and the base case is much higher than that of the higher viscosity case and the base case. The reason for that is the low gas viscosity does not deplete the reservoir pressure at the same rate as the higher gas viscosity because it would take much less pressure for the lower viscosity to initiate and maintain the gas flow. The pore pressure along the third fracture also shows that the difference ratio of the decoupled cases is higher than that of the coupled cases.

In the sensitivity analysis of the gas viscosity, the error margin of the simulation cases when the geomechanical effects were decoupled gets higher when the gas viscosity is reduced. The reason for that is that as the gas viscosity gets lower, it would take less pressure to derive it to flow, and because the decoupled cases do not account for the formation deformation, the pressure depletion seems to be less than the coupled cases.
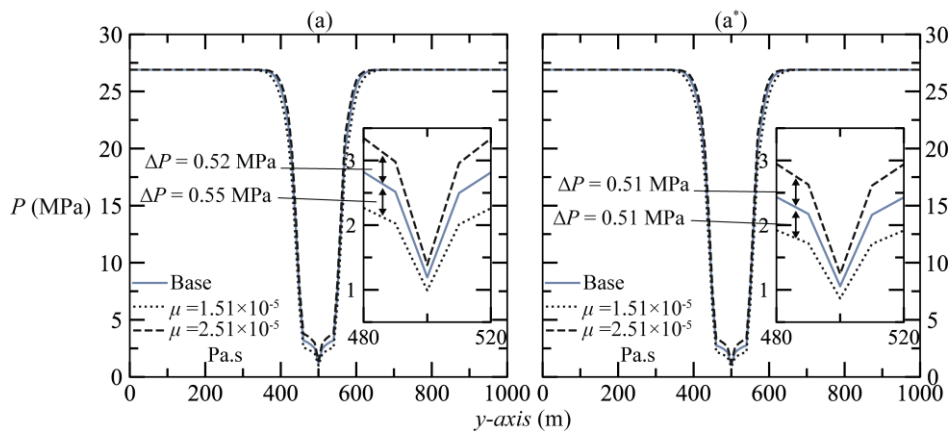
Fig. 6. Gas viscosity sensitivity analysis (a) the pore pressure along the third fracture for the decoupled case, and (a*) the pore pressure along the third fracture for the coupled case

3.2.2 SRV porosity

Figure 7(a) and (a*) show the production flow rate of the SRV porosity sensitivity analysis for the decoupled and coupled cases, respectively. Generally, Figure 7 shows that as the SRV porosity increases, the production flow rate increases and vice versa when the SRV porosity decreases. However, for the lower SRV porosity, the flow rate decline in the first 100 days is sharper in the coupled case compared to the decoupled case. That is because the coupled cases consider the rock deformation, which in the case of the lower SRV porosity, causes a further decrease in the porosity in general, leading to a sharp decline in the flow rate. However, for the case of the higher SRV viscosity compared to the base case, the difference ratio in the coupled case seems to be higher than that of the decoupled case. However, if the coupled case is to be compared with the decoupled case, the decoupled case still overestimates the production flow rate.

Figure 7(b) and (b*) show the cumulative production for the SRV porosity sensitivity analysis for the decoupled and coupled cases, respectively. The coupled cases in Figure 7(b*) show that the cumulative production difference ratio between the base case and the two SRV porosity cases is more significant when compared to the decoupled cases shown in Figure 7(b*). For the lower SRV porosity in the coupled case, the difference in cumulative production is about 1.58×10^4 m^3 which is about a 28.7% decrement. However, in the decoupled case, the difference between the base case and the lower SRV porosity is about 9.2×10^4 m^3, which is only about a 14.9% decrement. This shows that if the porosity of the SRV were less than that used in the base case, the cumulative production difference between the coupled and the decoupled cases would be about 1.35×10^4 m^3, which almost double the difference of that in the base case that is shown in Figure 3(b). This shows that when the geomechanics effects were decoupled from the reservoir simulator, the simulator greatly overestimated the production flow rate and the cumulative production. Consequently, the less the porosity, the more the error margin would be if the geomechanics effects were decoupled.

On the one hand, the difference between the higher SRV porosity and the base case in the coupled simulation case is about 1.33×10^4 m^3 which is about a 24.2% increment. On the other hand, the difference between the base case and the higher SRV porosity for the decoupled cases is about 1.02×10^4 m^3, which is about a 16.4% increment. In addition, if the coupled and decoupled cases were compared, the difference for the higher SRV porosity would be about 3.7×10^3 m^3, which is about half of that in the base cases that are shown in Figure 3(b). Consequently, the higher the porosity, the less the error margin would be if the geomechanics effects were decoupled.
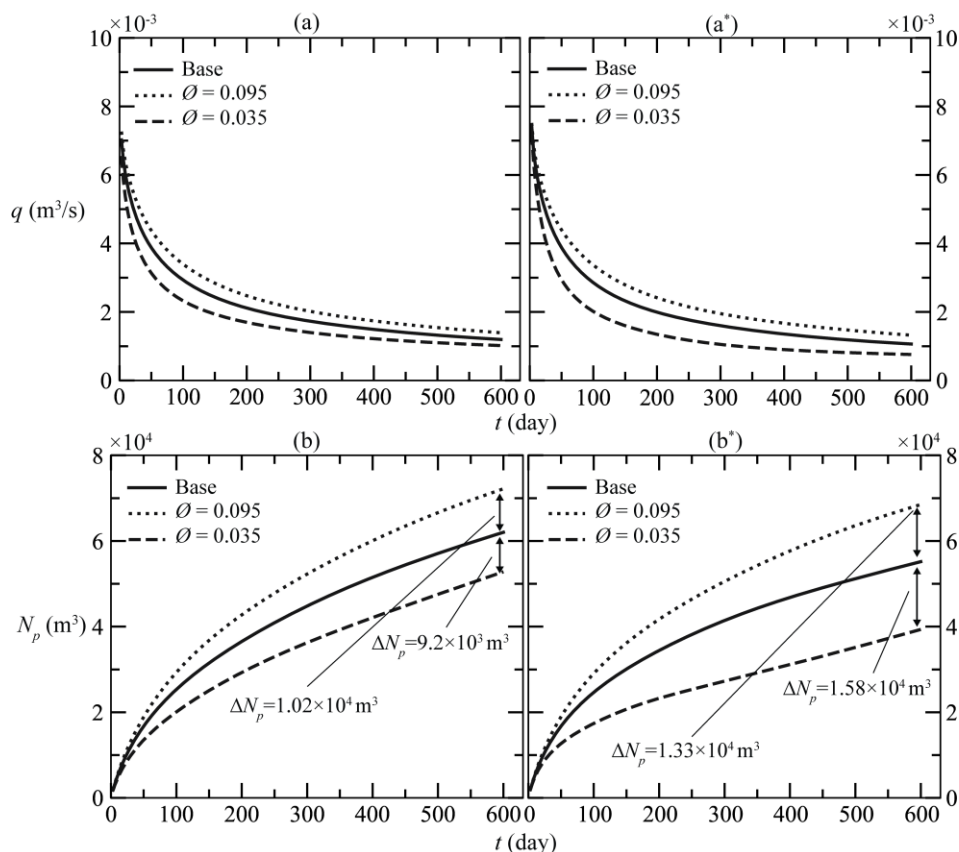
Fig. 7. SRV porosity sensitivity analysis, (a) the flow rate of the decoupled case, (a*) the flow rate for the coupled case, (b) the cumulative production for the decoupled case, and (b*) the cumulative production for the coupled case

Figure 8(a) and (a*) show the pore pressure profile along the third fracture after 600 days of production for the decoupled and the coupled cases, respectively. Overall, the lower the SRV porosity, the higher the pressure depletion along the third fracture when approaching the well location. The reason is that the less the SRV porosity, the faster the pressure depletes. For the case of the lower SRV porosity and coupled simulation, the pore pressure along the third fracture shows a significant difference, not only when getting closer to the well but for the pressure depletion extension in the SRV region. The pressure depletion in the decoupled case extended in the SRV for about 50 meters more than the coupled case for the lower SRV porosity case. This explains the overestimation of the production flow rate and the cumulative production in the decoupled case. In addition, the coupled cases generally showed a higher-pressure depletion when compared to the decoupled cases. Also, in the coupled case, the pore pressure difference between the base case and the two SRV porosity cases is higher than that of the decoupled cases.
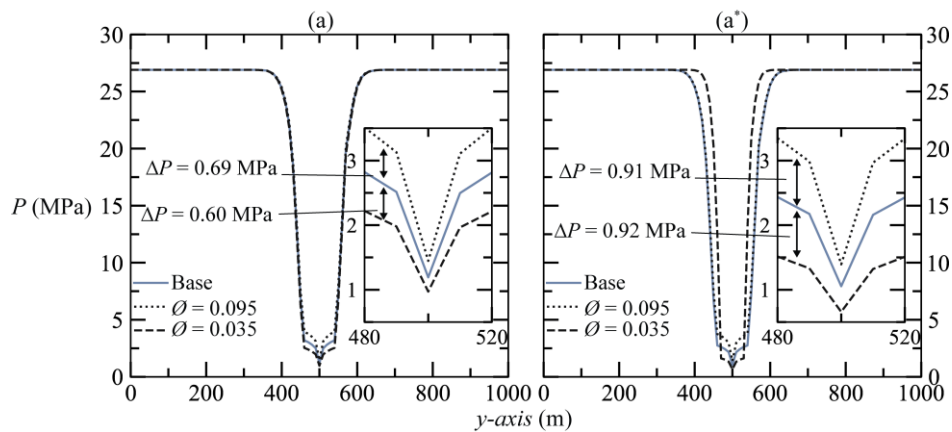
Fig. 8. SRV porosity sensitivity analysis (a) the pore pressure along the third fracture for the decoupled case, and (a*) the pore pressure along the third fracture for the coupled case

3.2.3 Fracture conductivity

Figure 9(a) and (a*) show the fracture conductivity sensitivity analysis for the decoupled and coupled cases, respectively. Overall, as the fracture conductivity increased, the production flow rate increased, and vice versa. Additionally, the flow rate difference in the fracture conductivity sensitivity analysis seems to be the most significant among the three sensitivity analyses carried out in this study. The reason is that hydraulic fractures are the main conduits for fluid flow in shale formations. As a result, any enhancement to the fracture conductivity would potentially enhance the overall production flow rate and cumulative production. The lower fracture conductivity cases show a significant decrease in production flow rate compared to the base cases in both the coupled and the decoupled cases. The magnitude of the flow rate decline in the lower fracture conductivity with respect to time is not as high as that of the base cases and the higher fracture conductivity cases.

Figure 9(b) and (b*) show the cumulative production of the fracture conductivity sensitivity analysis for the decoupled and coupled cases, respectively. From Figure 9(b) and (b*), the difference between the cases of different fracture conductivity is shown to be more notable. In the coupled case shown in Figure 9(b*), the difference between the base case and the lower fracture conductivity case is about 4.44×10^4 m³, which is about an 80.5% decrement. However, in the decoupled case shown in Figure 9(b), the difference between the base and the lower fracture conductivity cases is about 4.94×10^4 m³, which is about a 79.6% decrement. Meanwhile, in the decoupled cases, the difference between the lower fracture conductivity case and the base case is lower than that of the coupled cases, and the overall cumulative production in the decoupled case is still higher than that of the coupled case. This shows that the decoupled simulation still overestimates the cumulative production by about 1.9×10^3 m³, which is 72% less overestimation when compared to the difference shown in Figure 3(b).

In the coupled case shown in Figure 9(b*), the difference between the base case and the higher fracture conductivity case is about 2.22×10^4 m³, which is about a 40.2% increment. However, in the decoupled case shown in Figure 9(b), the difference between the base case and the higher fracture conductivity case is about 2.35×10^4 m³, which is about 37.8%. It is clear from Figure 9(b) and (b*) that the higher fracture conductivity case in the decoupled simulation still overestimates the cumulative production by about 8.1×10^3 m³, which is about 16% increment of overestimation when compared to the difference shown in Figure 3(b). This shows that as the fracture conductivity increase, the error margin in the decoupled cases also increases.
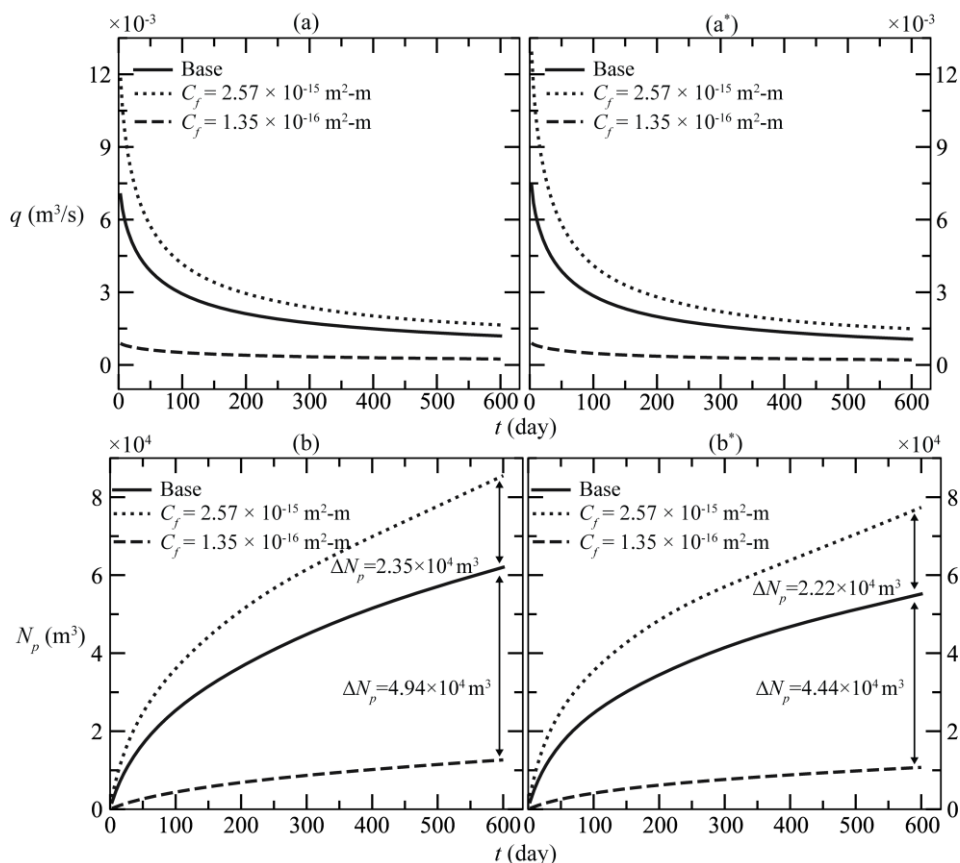
Fig. 9. Fracture conductivity sensitivity analysis, (a) the flow rate of the decoupled case, (a*) the flow rate for the coupled case, (b) the cumulative production for the decoupled case, and (b*) the cumulative production for the coupled case

Figure 10(a) and (a*) show the fracture conductivity sensitivity analysis for the pore pressure along the third fracture after 600 days of production for the decoupled and coupled cases, respectively. In the sensitivity analysis of the fracture conductivity, the decoupled cases still show less pressure depletion compared to the coupled simulation cases. For both the coupled and decoupled cases, it is shown that the cases of the higher fracture conductivity deplete the pore pressure more than that of the lower fracture conductivity cases. This happens because when the fracture conductivity is higher, the gas is allowed to flow faster, as shown in Figure 9(a) and (a*), which leads to higher pressure depletion. For the cases of the lower fracture conductivity, the pore pressure still shows a less depletion profile when compared to the base cases and higher conductivity cases for both the couple and the decoupled cases. This occurs because the low fracture conductivity reduces the flow rate of the gas, which in turn, keeps the pore pressure maintained. This is also shown in Figure 9(a) and (a*), where the decline of the flow rate with time is not as high as that of the base and higher fracture conductivity cases.

Generally, in the sensitivity analysis carried out in this study, it can be concluded that as the viscosity is lower, the porosity is higher, and the fracture conductivity is higher, the horizontal well shows a better production performance and vice versa. However, it is important to note that when geomechanical effects were decoupled from the reservoir simulator, the numerical results might be misleading, especially in the case of extremely low porosity. That is because the decoupled simulation overestimates the production flow rate and cumulative production and shows that the pore pressure is still maintained. Therefore, using the decoupled simulation in stress-sensitive formations with low

porosity and low permeability would result in erroneous flow rate estimations and might adversely affect field development plans.

It is also important to note that for formations with high porosity, the margin error of using decoupled simulations might be less than that when used for extremely low porosity formations. However, the error margin would always be there. In addition, when the geomechanical effects are coupled with the reservoir simulator, the pore pressure prediction seems more realistic compared to the cases when the geomechanical effects were decoupled.
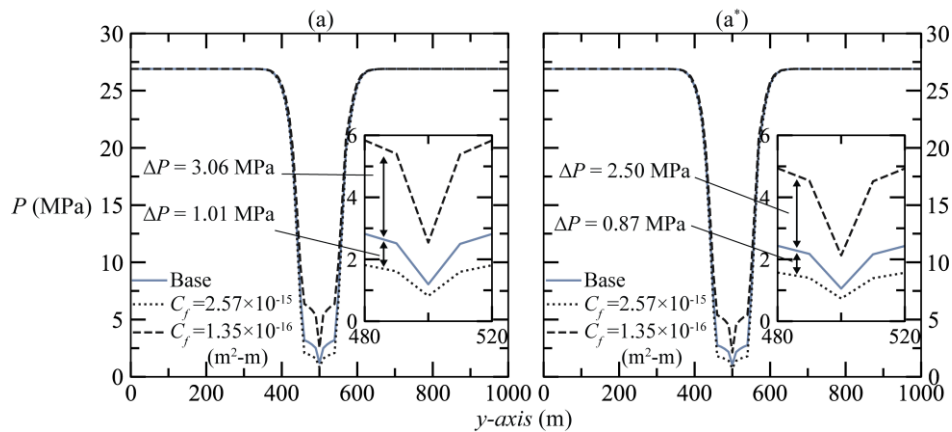

Fig. 10. Fracture conductivity sensitivity analysis (a) the pore pressure along the third fracture for the decoupled case, and (a*) the pore pressure along the third fracture for the coupled case

4. Conclusion

Significant hydrocarbon production from shale rock formations has emerged lately. However, shale formations are well known for being stress sensitive. As a result, using the conventional reservoir simulators that use constant rock compressibility to denote rock deformation does not accurately predict the production flow rate and the pore pressure depletion in the reservoir. Consequently, it is important to include the rock's mechanical properties in the reservoir simulator. In order to do that, the coupling of fluid flow in porous media with the geomechanics must be used to simulate hydrocarbon production from such formations. However, when such a numerical approach is used to study the production from shale formations, the fluid properties and the reservoir petrophysical properties are usually overlooked. This paper presents a sensitivity analysis of a single horizontal well performance using a fully coupled fluid flow and geomechanics model. The sensitivity analysis is carried out for the gas viscosity, SRV porosity, and fracture conductivity. The results are then compared for the cases when the geomechanical effects were coupled and decoupled with the reservoir simulator.

For both cases, when the geomechanical effects were coupled and decoupled, the production performance of the horizontal well was improved when the gas viscosity was lower than the base case, and it was impaired when the gas viscosity was higher than the base case. The horizontal well production was also enhanced when the SRV porosity was greater than that of the base case, and the production performance declined when the SRV porosity was reduced below the base case. In addition, when the fracture conductivity was higher than that of the base case, the production performance of the horizontal well seemed to improve. However, the production performance was greatly impaired when the fracture conductivity was below that of the base case.

Generally, in the sensitivity analysis conducted in this study, when the geomechanical effects were decoupled, the reservoir simulator seemed to overestimate the production flow rate and the cumulative production. It also tends to underestimate the pore pressure depletion along the hydraulic fractures. The results showed that when the SRV porosity was extremely low, the decoupled simulation case greatly overestimated the production flow rate and the cumulative production compared to other parameters in the sensitivity analysis conducted in this study. As a result, for a more accurate estimation of the production profile and cumulative production of a well in a stress-sensitive formation such as shale formations, it is advised that geomechanical effects are coupled with the reservoir simulator, especially if the porosity is extremely low.

Acknowledgment

References

[1] Mikayilov, Jeyhun I., Shahriyar Mukhtarov, Hasan Dinçer, Serhat Yüksel, and Rıdvan Aydın. "Elasticity Analysis of Fossil Energy Sources for Sustainable Economies: A Case of Gasoline Consumption in Turkey." *Energies* 13 no. 3 (2020): 731. https://doi.org/10.3390/EN13030731

[2] Ovezmyradov, Berdymyrat, and Yolbars Kepbanov. "Dependence of Central Asian Countries on Fossil Energy and Low Adoption of Non-Hydro Renewables." *SSRN Electronic Journal* (2022). https://doi.org/10.2139/SSRN.4193407.

[3] Abdullahi, M.B., S.R. Jufar, S. Kumar, T.M. Al-shami, and B.M Negash. "Synergistic Effect of Polymer-Augmented Low Salinity Flooding for Oil Recovery Efficiency in Illite-Sand Porous Media." *Journal of Molecular Liquids* 358 (2012): 119217. https://doi.org/10.1016/J.MOLLIQ.2022.119217

[4] Abdullahi, Mohammed Bashir, Shiferaw Regassa Jufar, Iskandar Dzulkarnain, Tareq Mohammed Al-shami, and Minh Duc Le. "Seismic Wave Excitation of Mature Oil Reservoirs for Green EOR Technology." *Journal of Advanced Research in Fluid Mechanics and Thermal Sciences* 103, no. 2 (2023): 180–96. https://doi.org/10.37934/ARFMTS.103.2.180196

[5] Caineng, Zou, Yang Zhi, Zhang Guosheng, Hou Lianhua, Zhu Rukai, Tao Shizhen, Yuan Xuanjun, et al. "Conventional and Unconventional Petroleum' Orderly Accumulation': Concept and Practical Significance." *Petroleum Exploration and Development* 41, no. 1 (2014): 14–30. https://doi.org/10.1016/S1876-3804(14)60002-1

[6] Muther, Temoor, Haris Ahmed Qureshi, Fahad Iqbal Syed, Hassan Aziz, Amaar Siyal, Amirmasoud Kalantari Dahaghi, and Shahin Negahban. "Unconventional Hydrocarbon Resources: Geological Statistics, Petrophysical Characterization, and Field Development Strategies." *Journal of Petroleum Exploration and Production Technology* 12 (2021):1–26. https://doi.org/10.1007/S13202-021-01404-X

[7] Rahman, Musfika, and Iskandar Dzulkarnain. "RSM for Modelling the CO2 Effect in the Interfacial Tension Between Brine and Waxy Dulang Crude Oil During LSW-WAG EOR." *Journal of Advanced Research in Fluid Mechanics and Thermal Sciences* 85, no. 2 (2021): 159–74. https://doi.org/10.37934/ARFMTS.85.2.159174

[8] Dhir, Ravindra K., Jorge de Brito, Raman Mangabhai, and Chao Qun Lye. "Use of Copper Slag in Geotechnical Applications." *Sustainable Construction Materials: Copper Slag*, January (2017):211–45. https://doi.org/10.1016/B978-0-08-100986-4.00006-7

[9] Abdulelah, Hesham, Berihun Mamo Negash, Nurudeen Yekeen, Sameer Al-Hajri, Eswaran Padmanabhan, and Ahmed Al-Yaseri. "Synergetic Effect of Surfactant Concentration, Salinity, and Pressure on Adsorbed Methane in Shale at Low Pressure: An Experimental and Modeling Study." *ACS Omega* 5, no. 32 (2020): 20107–21. https://doi.org/10.1021/ACSOMEGA.0C01738

[10] Abdulelah, Hesham, Syed M. Mahmood, and Ahmed Al-Mutarreb. "Effect of Anionic Surfactant on Wettability of Shale and Its Implication on Gas Adsorption/Desorption Behavior." *Energy and Fuels* 32, no. 2 (2018): 1423–32. https://doi.org/10.1021/ACS.ENERGYFUELS.7B03476

[11] Ziarani, Ali S., Roberto Aguilera, and Albert X. Cui. "Permeability of Tight Sand and Shale Formations: A Dual Mechanism Approach for Micro and Nanodarcy Reservoirs." *Society of Petroleum Engineers - SPE Canada Unconventional Resources Conference 2020,* OnePetro (2020). https://doi.org/10.2118/200010-MS

[12] Al-Shami, Tareq Mohammed, Shiferaw Regassa Jufar, Sunil Kumar, Hesham Abdulelah, Mohammed Bashir Abdullahi, Sameer Al-Hajri, and Berihun Mamo Negash. "A Comprehensive Review of Interwell Interference in Shale Reservoirs." *Earth-Science Reviews* 237 (2023): 104327. https://doi.org/10.1016/J.EARSCIREV.2023.104327

[13] Al-Hajri, Sameer, Berihun M. Negash, Md Motiur Rahman, Mohammed Haroun, and Tareq M. Al-Shami.

"Perspective Review of Polymers as Additives in Water-Based Fracturing Fluids," *ACS Omega* 7, no. 9 (2022):7431–7443. https://doi.org/10.1021/ACSOMEGA.1C06739

[14] Abdulelah, Hesham, Berihun Mamo Negash, Atta Dennis Yaw, Tareq M. Al-Shami, Ahmed Al-Yaseri, and Eswaran Padmanabhan. "Application of Benchtop Humidity and Temperature Chamber in the Measurement of Water Vapor Sorption in US Shales from Mancos, Marcellus, Eagle Ford and Wolfcamp Formations." *Journal of Petroleum Exploration and Production Technology* 12, no. 12 (2022): 2679–89. https://doi.org/10.1007/S13202-022-01465-6/TABLES/4

[15] JIA, Chengzao. "Breakthrough and Significance of Unconventional Oil and Gas to Classical Petroleum Geology Theory." *Petroleum Exploration and Development* 44, no. 1 (2017): 1–10. https://doi.org/10.1016/S1876-3804(17)30002-2

[16] JIAO, Fangzheng. "Re-Recognition of 'Unconventional' in Unconventional Oil and Gas." *Petroleum Exploration and Development* 46, no. 5 (2019): 847–55. https://doi.org/10.1016/S1876-3804(19)60244-2

[17] Al-Shami, Tareq Mohammed, Shiferaw Regassa Jufar, Berihun Mamo Negash, and Mohammed Bashir Abdullahi. "Impact of External Excitation on Flow Behavior of Trapped Oil Blob." *Journal of Petroleum Science and Engineering* 196 (2021): 108002. https://doi.org/10.1016/j.petrol.2020.108002

[18] Al-Shami, T. M., S. R. Jufar, Ghareb Mostafa Hamada, Dinesh A/L Kanesan, and U. Djuraev. "Effect of Seismic Excitation on Mobilization of Trapped Oil Globule in Pore Doublet Model." *International Journal of Mechanical Engineering and Robotics Research* 8, no. 6 (2019): 998–1002. https://doi.org/10.18178/ijmerr.8.6.998-1002

[19] Yang, Yun, and Shimin Liu. "Review of Shale Gas Sorption and Its Models." *Energy & Fuels* 34, no. 12 (2020): 15502–24. https://doi.org/10.1021/ACS.ENERGYFUELS.0C02906

[20] Lin, Wen. "A Review on Shale Reservoirs as an Unconventional Play – The History, Technology Revolution, Importance to Oil and Gas Industry, and the Development Future." *Acta Geologica Sinica - English Edition* 90, no. 5 (2016): 1887–1902. https://doi.org/10.1111/1755-6724.12823

[21] Abdulelah, Hesham, Berihun Mamo Negash, Tareq M. Al-Shami, Firas A. Abdulkareem, Eswaran Padmanabhan, and Ahmed Al-Yaseri. "Mechanism of CH4 Sorption onto a Shale Surface in the Presence of Cationic Surfactant." *Energy & Fuels* 35, no. 9 (2021): 7943–55. https://doi.org/10.1021/ACS.ENERGYFUELS.1C00613

[22] Al-Hajri, Sameer, Berihun M. Negash, Md Motiur Rahman, Mohammed Haroun, and Tareq M. Al-Shami. "Effect of Silica Nanoparticles on Polymer Adsorption Reduction on Marcellus Shale." *ACS Omega* 6, no. 44 (2021): 29537–29546. https://doi.org/10.1021/ACSOMEGA.1C03653

[23] Wu, Dawei, Yuan Di, and Yu-Shu Wu. "Coupled Geomechanics and Flow Modeling of Fractured Reservoirs Considering Matrix Permeability Anisotropy." *Geofluids* 2022 (2022): 1–25. https://doi.org/10.1155/2022/1200012

[24] Javadpour, F. "Nanopores and Apparent Permeability of Gas Flow in Mudrocks (Shales and Siltstone)." *Journal of Canadian Petroleum Technology* 48, no. 8 (2009): 16–21. https://doi.org/10.2118/09-08-16-DA

[25] Javadpour, F., D. Fisher, and M. Unsworth. "Nanoscale Gas Flow in Shale Gas Sediments." *Journal of Canadian Petroleum Technology* 46, no. 10 (2007): 55–61. https://doi.org/10.2118/07-10-06

[26] Warpinski, N. R., M. J. Mayerhofer, M. C. Vincent, C. L. Cipolla, and E. R. Lolon. "Stimulating Unconventional Reservoirs: Maximizing Network Growth While Optimizing Fracture Conductivity." *Journal of Canadian Petroleum Technology* 48, no. 10 (2009): 39–51. https://doi.org/10.2118/114173-PA

[27] Soliman, M. Y., and C. S. Kabir. "Testing Unconventional Formations." *Journal of Petroleum Science and Engineering* 92–93 (2012): 102–9. https://doi.org/10.1016/j.petrol.2012.04.027

[28] Jiang, Jiamin, and Jie Yang. "Coupled Fluid Flow and Geomechanics Modeling of Stress-Sensitive Production Behavior in Fractured Shale Gas Reservoirs." *International Journal of Rock Mechanics and Mining Sciences* 101 (2018): 1–12. https://doi.org/10.1016/j.ijrmms.2017.11.003

[29] Ferrari, Alessio, Valentina Favero, and Lyesse Laloui. "One-Dimensional Compression and Consolidation of Shales." *International Journal of Rock Mechanics and Mining Sciences* 88 (2016): 286–300. https://doi.org/10.1016/J.IJRMMS.2016.07.030

[30] Shovkun, Igor, and D. Nicolas Espinoza. "Coupled Fluid Flow-Geomechanics Simulation in Stress-Sensitive Coal and Shale Reservoirs: Impact of Desorption-Induced Stresses, Shear Failure, and Fines Migration." *Fuel* 195 (2017): 260–72. https://doi.org/10.1016/j.fuel.2017.01.057

[31] Wei, Chenji, Liangang Wang, Baozhu Li, Lihui Xiong, Shuangshuang Liu, Jie Zheng, Suming Hu, and Hongqing Song. "A Study of Nonlinear Elasticity Effects on Permeability of Stress Sensitive Shale Rocks Using an Improved Coupled Flow and Geomechanics Model: A Case Study of the Longmaxi Shale in China." *Energies* 11, no. 2 (2018): 329. https://doi.org/10.3390/en11020329

[32] Bataee, Mahmood, and Sonny Irawan. "Review of Geomechanical Application in Reservoir Modeling." *Journal of Applied Sciences* 14, no. 10 (2014): 981–90. https://doi.org/10.3923/jas.2014.981.990

[33] Kim, J., G. J. Moridis, D. Yang, and J. Rutqvist. "Numerical Studies on Two-Way Coupled Fluid Flow and Geomechanics in Hydrate Deposits." *SPE Journal* 17, no. 2 (2012): 485–501. https://doi.org/10.2118/141304-PA

[34] Terzaghi, K. "KDie Berechnung Der Durchlassigkeitsziffer Des Tones Aus Dem Verlauf Der Hidrodynamichen Span-Nungserscheinungen Akademie Der Wissenschaften." *Akademie Der Wissenschaften in Wien. Sitzungsberichte* 11 (1923): 105–24.

[35] Terzaghi, K. "Erdbaumechanik auf bodenphysikalischer Grundlage (Mechanics of earthworks based on rudiments of soil physics)." *Deuticke* (1925).

[36] Biot, M.A., and D.G. Willis. "The Elastic Coefficients of the Theory of Consolidation." *Journal of Applied Mechanics* 24 (1957): 594–601.

[37] Biot, M. A. "Theory of Elasticity and Consolidation for a Porous Anisotropic Solid." *Journal of Applied Physics* 26, no. 2 (1955): 182–85. https://doi.org/10.1063/1.1721956

[38] Biot, M.A. "General Theory of Three-Dimensional Consolidation." *Journal of Applied Physics* 12, no. 2 (1941): 155–64. https://doi.org/10.1063/1.1712886

[39] Geertsma, J. "Problems of Rock Mechanics In Petroleum Production Engineering." In *1st ISRM Congress*. Lisbon, Portuga: International Society for Rock Mechanics and Rock Engineering (1966)

[40] Huang, Jian, and Ahmad Ghassemi. "A Poroelastic Model for Evolution of Fractured Reservoirs during Gas Production." *Journal of Petroleum Science and Engineering* 135 (2015): 626–44. https://doi.org/10.1016/J.PETROL.2015.10.007

[41] Rutqvist, Jonny. "The Geomechanics of CO 2 Storage in Deep Sedimentary Formations." *Geotechnical and Geological Engineering* 30, no. 3 (2012): 525–51. https://doi.org/10.1007/S10706-011-9491-0

[42] Elyasi, Ayub, Kamran Goshtasbi, and Hamid Hashemolhosseini. 2016. "A Coupled Geomechanical Reservoir Simulation Analysis of CO_2 - EOR: A Case Study." *Geomechanics and Engineering* 10, no. 4 (2016): 423–36. https://doi.org/10.12989/GAE.2016.10.4.423

[43] Chin, L. Y., and L. K. Thomas. "Fully Coupled Analysis of Improved Oil Recovery by Reservoir Compaction." In *Proceedings - SPE Annual Technical Conference and Exhibition*. OnePetro (1999). https://doi.org/10.2523/56753-ms

[44] Dean, R. H., and J. H. Schmidt. "Hydraulic-Fracture Predictions with a Fully Coupled Geomechanical Reservoir Simulator." *SPE Journal* 14, no. 4 (2009): 707–14. https://doi.org/10.2118/116470-PA

[45] Guo, Xuyang, Hongqing Song, Kan Wu, and John Killough. "Pressure Characteristics and Performance of Multi-Stage Fractured Horizontal Well in Shale Gas Reservoirs with Coupled Flow and Geomechanics." *Journal of Petroleum Science and Engineering* 163 (2018): 1–15. https://doi.org/10.1016/j.petrol.2017.12.038

[46] Liu, Yongzan, Lijun Liu, Juliana Y. Leung, and George J. Moridis. "Sequentially Coupled Flow and Geomechanical Simulation with a Discrete Fracture Model for Analyzing Fracturing Fluid Recovery and Distribution in Fractured Ultra-Low Permeability Gas Reservoirs." *Journal of Petroleum Science and Engineering* 189 (2020): 107042. https://doi.org/10.1016/j.petrol.2020.107042

[47] Minkoff, Susan E., C.Mike Stone, Steve Bryant, Malgorzata Peszynska, and Mary F. Wheeler. "Coupled Fluid Flow and Geomechanical Deformation Modeling." *Journal of Petroleum Science and Engineering* 38, no. 1-2 (2003): 37–56. https://doi.org/10.1016/S0920-4105(03)00021-4

[48] Moradi, Mostafa, Amir Shamloo, and Alireza Daneh Dezfuli. "A Sequential Implicit Discrete Fracture Model for Three-Dimensional Coupled Flow-Geomechanics Problems in Naturally Fractured Porous Media." *Journal of Petroleum Science and Engineering* 150 (2017): 312–22. https://doi.org/10.1016/j.petrol.2016.12.027

[49] Hubbert, M. K. "Darcy's Law and the Field Equations of the Flow of Underground Fluids." *International Association of Scientific Hydrology. Bulletin* 2, no. 1 (1957): 23–59. https://doi.org/10.1080/02626665709493062

[50] Zhang, Chao, Sadiq J Zarrouk, and Rosalind Archer. "Development of a Fully Coupled Flow-Geomechanics Simulator for Flow in Saturated Porous Media." In *The International Conference on Computational Methods*. Auckland, New Zealand (2015).

[51] Ferronato, Massimiliano, Nicola Castelletto, and Giuseppe Gambolati. "A Fully Coupled 3-D Mixed Finite Element Model of Biot Consolidation." *Journal of Computational Physics* 229, no. 12 (2010): 4813–30. https://doi.org/10.1016/J.JCP.2010.03.018

[52] Yang, Daegil, George J. Moridis, and Thomas A. Blasingame. "A Fully Coupled Multiphase Flow and Geomechanics Solver for Highly Heterogeneous Porous Media." *Journal of Computational and Applied Mathematics* 270 (2014): 417–32. https://doi.org/10.1016/j.cam.2013.12.029

[53] Haagenson, Ryan, Harihar Rajaram, and Jeffery Allen. "A Generalized Poroelastic Model Using FEniCS with Insights into the Noordbergum Effect." *Computers & Geosciences* 135 (2020): 104399. https://doi.org/10.1016/j.cageo.2019.104399

[54] Soeder, D. J., and P. L. Randolph. "Porosity, Permeability, and Pore Structure of the Tight Mesaverde Sandstone, Piceance Basin, Colorado." *SPE Formation Evaluation* 2, no. 02 (1987): 129–36. https://doi.org/10.2118/13134-PA

[55] McKee, C. R., A. C. Bumb, and R. A. Koenig. "Stress-Dependent Permeability and Porosity of Coal and Other Geologic Formations." *SPE Formation Evaluation* 3, no. 01 (1988): 81–91. https://doi.org/10.2118/12858-PA

[56] Geertsma, J. "The Effect of Fluid Pressure Decline on Volumetric Changes of Porous Rocks." *Transactions of the AIME* 210, no. 01 (1957): 331–40. https://doi.org/10.2118/728-G

[57] Wei, K. K., N. R. Morrow, and K. R. Brower. "Effect of Fluid, Confining Pressure, and Temperature on Absolute Permeabilities of Low- Permeability Sandstones." *SPE Formation Evaluation* 1, no. 04 (1986): 413–23. https://doi.org/10.2118/13093-PA

[58] Dobrynin, Valery M. "Effect of Overburden Pressure on Some Properties Of Sandstones." *Society of Petroleum Engineers Journal* 2, no. 04 (1962): 360–66. https://doi.org/10.2118/461-PA

[59] Davies, J.P., and D.K. Davies. 1999. "Stress-Dependent Permeability: Characterization and Modeling." In *SPE Annual Technical Conference and Exhibition*. Society of Petroleum Engineers (1999). https://doi.org/10.2118/56813-MS

[60] Alnaes, Martin S, Jan Blechta, Johan Hake, August Johansson, Benjamin Kehlet, Anders Logg, Chris Richardson, Johannes Ring, Marie E Rognes, and Garth N Wells. "The FEniCS Project Version 1.5." *The FEniCS Project Version 1.5* 3, no. 100 (2015): 9–23. https://doi.org/10.11588/ans.2015.100.20553

[61] Logg, Anders, and Garth N. Wells. "DOLFIN: Automated Finite Element Computing." *ACM Transactions on Mathematical Software* 37, no. 2 (2010): 1–28. https://doi.org/10.1145/1731022.1731030

[62] Kirby, Robert C. "Algorithm 839." *ACM Transactions on Mathematical Software (TOMS)* 30, no. 4 (2004): 502–16. https://doi.org/10.1145/1039813.1039820

[63] Kirby, Robert C., and Anders Logg. "A Compiler for Variational Forms." *ACM Transactions on Mathematical Software (TOMS)* 32, no. 3 (2006): 417–44. https://doi.org/10.1145/1163641.1163644

[64] Alnaes, Martin S., Anders Logg, Kristian B. Oelgaard, Marie E. Rognes, and Garth N. Wells. "Unified Form Language: A Domain-Specific Language for Weak Formulations of Partial Differential Equations." *ACM Transactions on Mathematical Software* 40, no. 2 (2012). http://arxiv.org/abs/1211.4047

[65] Abhyankar, Shrirang, Jed Brown, Emil M. Constantinescu, Debojyoti Ghosh, Barry F. Smith, and Hong Zhang. 2018. "PETSc/TS: A Modern Scalable ODE/DAE Solver Library," (2018). https://doi.org/10.48550/arxiv.1806.01437

[66] Verruijt, Arnold. "Consolidation of Soils." In *Encyclopedia of Hydrological Sciences*. Chichester, UK: John Wiley & Sons, Ltd (2008). https://doi.org/10.1002/0470848944.hsa303

[67] Verruijt, Arnold. "Theory of Consolidation." In , 8–34. Springer, Dordrecht (1995).https://doi.org/10.1007/978-94-017-1112-8_2

[68] Song, Hongqing, Zhengyi Li, Yuhe Wang, Weiyao Zhu, Yang Cao, and John Killough. "A Novel Approach for Modeling Gas Flow Behaviors in Unconventional Reservoirs with Nanoporous Media." In *the International Petroleum Technology Conference 2015*. Society of Petroleum Engineers (2015). https://doi.org/10.2523/iptc-18316-ms

[69] Vermylen, John Peter. "Geomechanical Studies of the Barnett Shale, Texas, USA." Stanford University (2011).

[70] Yu, Wei, and Kamy Sepehrnoori. 2014. "Simulation of Gas Desorption and Geomechanics Effects for Unconventional Gas Reservoirs." *Fuel* 116 (2014): 455–64. https://doi.org/10.1016/j.fuel.2013.08.032

[71] Zoback, Mark D. *Reservoir Geomechanics*. *Reservoir Geomechanics*. Cambridge, New York: Cambridge University Press (2007). https://doi.org/10.1017/CBO9780511586477

[72] Ajisafe, Foluke O, Irina Solovyeva, Adrian Morales, Efe Ejofodomi, and Matteo Marongiu Porcu. 2017. "Impact of Well Spacing and Interference on Production Performance in Unconventional Reservoirs, Permian Basin." In *Unconventional Resources Technology Conference*, 16. https://doi.org/10.15530/URTEC-2017-2690466

[73] Lee, Anthony L, Mario H Gonzalez, Junior Members, Aime Bertram, and E Eakin. "The Viscosity of Natural Gases." *Journal of Petroleum Technology* 18, no. 08 (1966): 997–1000. https://doi.org/10.2118/1340-PA

[74] Carr, Norman L., Riki Kobayashi, and David B. Burrows. "Viscosity of Hydrocarbon Gases Under Pressure." *Journal of Petroleum Technology* 6, no. 10 (1954): 47–55. https://doi.org/10.2118/297-G

[75] Guo, Chaohua, Mingzhen Wei, and Hong Liu. "Modeling of Gas Production from Shale Reservoirs Considering Multiple Transport Mechanisms." Edited by Bing-Yang Cao. *PLOS ONE* 10, no. 12 (2015): e0143649. https://doi.org/10.1371/journal.pone.0143649

[76] Zhang, Junjing, Anton Kamenov, D. Zhu, and A. D. Hill. "Measurement of Realistic Fracture Conductivity in the Barnett Shale." *Journal of Unconventional Oil and Gas Resources* 11 (2015): 44–52. https://doi.org/10.1016/J.JUOGR.2015.05.002